Nanoscale Res Lett (2008) 3:6–13
DOI 10.1007/s11671-007-9106-0

NANO EXPRESS

Mechanical Deformation Induced in Si and GaN Under Berkovich Nanoindentation

Sheng-Rui Jian

Received: 3 September 2007 / Accepted: 12 November 2007 / Published online: 27 November 2007
© to the authors 2007

Abstract Details of Berkovich nanoindentation-induced mechanical deformation mechanisms of single-crystal Si(100) and the metal-organic chemical-vapor deposition (MOCVD) derived GaN thin films have been systematic investigated by means of micro-Raman spectroscopy and cross-sectional transmission electron microscopy (XTEM) techniques. The XTEM samples were prepared by using focused ion beam (FIB) milling to accurately position the cross-section of the nanoindented area. The behaviors of the discontinuities displayed in the loading and unloading segments of the load-displacement curves of Si and GaN thin films performed with a Berkovich diamond indenter tip were explained by the observed microstructure features obtained from XTEM analyses. According to the observations of micro-Raman and XTEM, the nanoindentation-induced mechanical deformation is due primarily to the generation and propagation of dislocations gliding along the pyramidal and basal planes specific to the hexagonal structure of GaN thin films rather than by indentation-induced phase transformations displayed in Si.

Keywords Si · GaN · Nanoindentation · Micro-Raman spectroscopy · Focused ion beam · Cross-sectional transmission electron microscopy

S.-R. Jian (✉)
Department of Materials Science and Engineering, I-Shou University, No.1, Sec.1, Syuecheng Rd., Dashu Township, Kaohsiung 840, Taiwan
e-mail: srjian@gmail.com

Introduction

The development of nanotechnology and microsystems has relied, in many ways, on the major progresses accomplished in surface science and materials science. In the past, much effort has been devoted to characterizing the optical, electrical, and magnetic characteristics of the resultant structures and devices. The successful fabrication of devices based on semiconductors requires better understanding of the mechanical characteristics in addition to their optical and electrical performances. This is because that the contact loading during processing or packaging can significantly degrade the performance of these devices. Therefore, there is a growing demand of investigating the mechanical characteristics of materials, in particular in the nanoscale regime, for device applications.

Contact loading is a type of mechanical impact that many electronic materials experience during processing or application, there are several issues to be addressed. Firstly, the mechanical responses of materials to an applied load might be vastly different from that of the same bulk ones. For this purpose, unfortunately, the traditional methods such as tensile measurements do not scale well into the micrometer- and nanometer-regions. Secondly, the role of structural changes under contact loading are largely underestimated owing to the difficulties in probing the structural characterizations of materials affected by the contact interaction directly. In this respect, depth-sensing indentation (nanoindentation) has proven to be a powerful technique in providing information on mechanical properties (hardness and elastic modulus) of materials and, variation of these properties with the penetration depth, based on the analysis of the respective load-displacement curves [1–6] while also producing contact-induced damage. While diamond anvil cell (DAC) experiments are

capable of investigating the mechanical and phase transformation in bulk materials under hydrostatic pressure [7], the materials behavior under nanoindentation is of more relevance to realistic contact loading conditions.

In fact, the load-displacement curves obtained during nanoindentation can be viewed as "fingerprints" that contain much information about deformation mechanisms. For example, the onset for dislocation slip or twinning event in InP and GaAs [8] and, the solid-state phase transformation in Si [9] have been associated with the discontinuities during nanoindentation. For GaN thin films, Bradby et al. [10–12] proposed the mechanical deformation behaviors during nanoindentation with the spherical indenter. During the nanoindentation of GaN thin films, a discontinuity (so-called "pop-in" event) in the loading curve was observed, indicating that the main deformation mechanism appears to be the nucleation of slip [12]. Nevertheless, the point indenter induced microstructural changes have not received sufficiently attention yet. As a result, locations of the details of single-crystal Si(100) and GaN thin films microstructure via a nanoindentation with a Berkovich diamond indenter have not been explored.

Herein, in this study, the deformation behaviors of single-crystal Si(100) and metal-organic chemical-vapor deposition (MOCVD)-deposited GaN thin films under contact loading have been investigated using Berkovich nanoindentation, followed by analysis using micro-Raman spectroscopy and cross-sectional transmission electron microscopy (XTEM) techniques, in order to understand the final structures of the indentation-induced transformation zones observed in experiments.

Experimental Details

Two materials of single-crystal Si(100) wafer with light boron doping (1×10^{15} atoms/cm^3) and, GaN thin films deposited on (0001)-sapphire substrates by using the metal-organic chemical vapor deposition (MOCVD) method with an average thickness of about 2 μm [3] were used in our present experiments.

The nanoindentation tests were performed on a Nano-indenter MTS NanoXP® system (MTS Cooperation, Nano Instruments Innovation Center, TN, USA) with a diamond pyramid-shaped Berkovich-type indenter tip (face angle 65.3°), whose radius of curvature is 50 nm.

For microstructure analyses, a 10×5 indent array with each indent separated by 100 μm was produced by holding at the peak load of 200 mN for 30 s with the same loading/unloading rates of 0.5 mN/s and 10 mN/s for single-crystal Si(100) and GaN thin films, respectively. The materials residual impressions produced at an indentation load of 200 mN were examined by a micro-Raman spectrometer (Renishaw, UK) with an Ar^+ laser (excitation wavelength 514.5 nm). The size of the laser spot is about 1 μm, smaller than the dimension of impressions $\sim$5 μm. In the Raman experiments, a low laser power of 2 mW was used to avoid any possible artifacts from the center of the residual impressions as determined by optical microscopy.

The cross-sectional transmission electron microscopy (XTEM) samples were prepared by means of a FEI Nova 220 Dual-Beam workstation—focused ion beam (FIB)/scanning electron microscopy (SEM) system. This technique enabled us to cut through the nanoindentation and locate the specific site of interesting efficiently. In practice, we first milled two crosses alongside the indented area for markers and, then deposited a 1 μm-thick Pt layer to protect this area of interest from Ga^+ ion beam damage and implantation. Material was removed from both sides of the selected area with an ion current of 5 nA, followed by successive thinning steps with decreasing current ranging from 3 nA to 300 pA until the lamella was about 1 μm-thick. Subsequently, the bottom and one side of the lamella were cut free while titling the sample at an angle of 45° to the ion beam. A central area containing the nanoindentation apex of a few micrometers in length was then chosen and thinned further to a thickness of $\sim$100 nm, leaving at the sides thicker areas that prevented the lamella from collapsing. An ion dose of 70 pA was adopted for final cleaning steps. Finally, a small area of interest was selected and thinned until electron transparency was achieved. The transfer of the lamella from the sample holder to a holey carbon coated TEM grid was made ex situ by using a shape glass tip under an optical microscope outside FIB station. A JEOL-2010 TEM operated at an accelerating voltage of 200 kV was used to study the microstructures of XTEM lamella.

Results and Discussion

Nanoindentation on Single-crystal Si(100)

Silicon (Si-I) is a technologically very important material and is also of considerable scientific interest for its electrical, mechanical structural and, optical characterizations. In the past four decades there have been a significant number of investigations of the structural phase transformations of Si when it is subjected to sufficiently high hydrostatic or non-hydrostatic pressures. It is well accepted from DAC high pressure studies that Si transforms from the cubic diamond phase (Si-I) to the metallic β-Sn phase (Si-II) at increased pressures [13, 14]. During pressure release Si-II further transforms into several metastable phases including amorphous silicon, body-centered-cubic Si-III phase, rhombohedral distortion Si-XII phase [15]

and, hexagonal diamond phase Si-IV [16]. These pressure-induced phase transitions can also be achieved by indentation tests [9, 17–21]. In addition, it has been demonstrated that the microstructures of Si after indentation with a spherical indenter depends on the maximum indentation load [9], loading/unloading rate [22] and, number of applied stress cycles [23]. And, a larger indentation load endorses crystalline phase transformation [24], while a high loading/unloading indentation rate promotes an amorphous phase [22].

Since phase transformations significantly affect the electrical, optical and mechanical characteristics of machined surface, the machining processes also have important implications for the manufacture of Si substrates, microelectromechanical systems and, microelectronics devices. Nevertheless, the Berkovich indenter induced microstructural changes have not received sufficient attention. Moreover, the plan-view TEM analyses cannot distinguish the phase changes inside the deformation region along the vertical direction. Consequently, in this section, we will use the micro-Raman spectroscopy and cross-sectional view TEM techniques to clarify this problem mainly.

Figure 1 shows a typical indentation load-displacement curve of single-crystal Si(100) subjected to a maximum indentation load of 200 mN, corresponding to different phase transformations as suggested by Bradby et al. [9]. The sudden displacement discontinuities, the pop-ins and pop-out phenomena, were observed in the loading and unloading part, respectively. Association of pop-in events with the onset of Si-I to Si-II phase transformation was reported recently in [9], which suggested that phase transformation begins at earlier stages of loading and pop-in is simple a manifestation of the sudden extrusion of highly plastic transformed materials from underneath the indenter. And, there is agreement with the previous study [25] that upon unloading, the formation of Si-III and Si-XII is evidenced by pop-out event. This is supported by the results of phase characteristics within the residual indents, carried out primarily by using of Raman spectroscopy [25, 26] and TEM [9, 18, 22]. In addition, it can be found that only one major subsequent pop-in occurs during the indentation loading curve, there are obviously three cracking events along the corner of residual indentation (please see SEM micrograph in the insert of Fig. 1). Therefore, the cause of the subsequent pop-in event is attributed to the Berkovich indentation induced cracking on Si surface.

Figure 2 shows the micro-Raman spectra obtained from an indentation load of 200 mN presented in Fig. 1. In Fig. 2, the Raman spectra from a 200 mN nanoindentation on Si clearly reveal the additional bands at 160, 184, 350, 390, 433 and 486 cm^{-1}, commonly associated with the

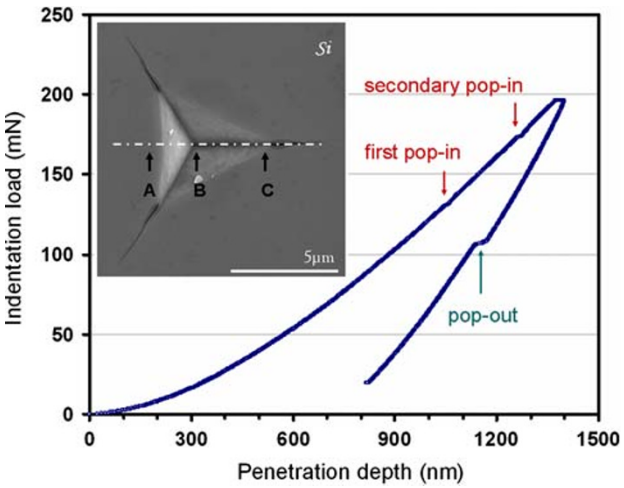

Fig. 1 Load-displacement data for single-crystal Si(100) obtained during nanoindentation with a Berkovich indenter showing two "pop-in" events during loading and, one "pop-out" event during unloading. And, the inset is a SEM micrograph showing the indentation at an applied load of 200 mN

Si-III and Si-XII phases [17]. The formation region of Si-III and Si-XII phases in center and corner of indentation is found to be much stronger than that in edge one, suggesting that the magnitude of shear stress in the central part is higher. Shear stress produced by indentation also plays a crucial role in determining which phases are formed [27]. As the metastable phases of Si-III and Si-XII can be formed only via a metallic Si-II phase, this observation suggests pressure-induced metallization of Si during nanoindentation [28] similar to the results of high-pressure cell experiments.

Figure 3 shows a XTEM bright-field image of a 200 mN indent in single-crystal Si(100). Characteristics "pop-out" event during unloading is seen in Fig. 2, which is thought to be associated with a phase transformation [9]. An amorphous phase is obvious in the upper part of the zone. Nevertheless, crystalline phases are located in the central part at the bottom of the transformation zone. At the tip of the nanoindentation-induced transformed zone a crack which extends below the surface is formed. Material from the transformed zone appears to have been extruded into the top of the crack, which is consistent with the formation of a ductile metallic phase under loading [26]. In addition, a selected area diffraction (SAD) of the region immediately beneath the residual indent (shown as an insert to this figure) shows that the nanoindentation-induced transformed zone is a mixture of amorphous and, some crystal materials (which are consistent with results from the previous study [24] as arising from the metastable phases of Si-III and Si-XII). The location of the crystalline phases is different from those formed in the previous work [29] with the spherical indenter. Also, the major difference between

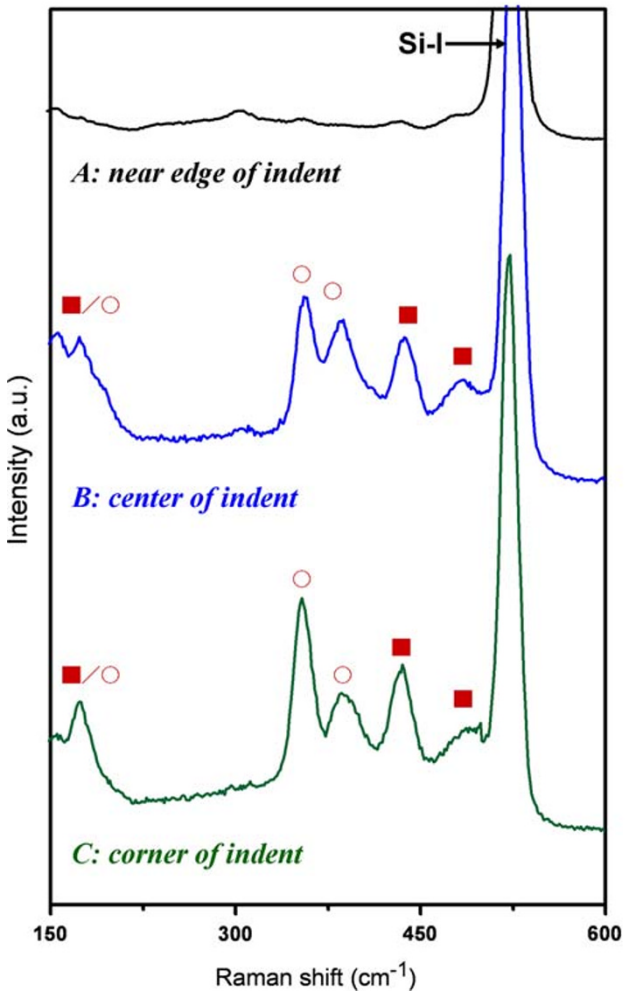

Fig. 2 Raman spectra taken from the Berkovich indentation of single-crystal Si(100) at the corner, the center and near edge of indent. Because of the nanoindentation-induced phase transformations, there are crystalline metastable phases present. (The symbols ■ and ○ are denoted as Si-III and Si-XII phases)

these two microstructures is the median crack that is formed under the indent made by Berkovich indenter whereas no cracking was observed in the indent subject to the spherical indentation [9].

In closing, we have made on indentation in single-crystal Si(100) to track the transformation of the metastable phases of Si-III and Si-XII using micro-Raman spectroscopy in combination with XTEM techniques. Multiple pop-ins and pop-out events on Si have been reported; the cause of the pop-ins is not clear at this time, but the pop-out is ascribed to the reason of phase transformation. Micro-Raman spectroscopy demonstrated its ability to detect phase changes beneath the Si surface, giving different signature at different location surrounding the indentation. The extra Raman bands from the metastable phases of

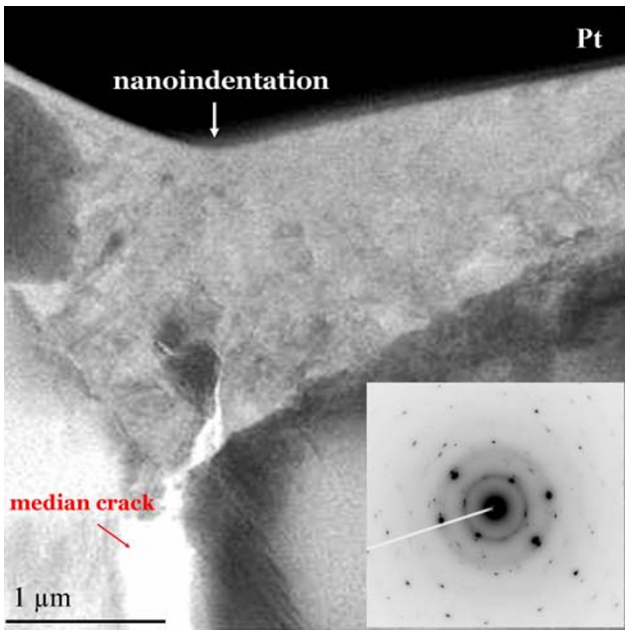

Fig. 3 The bright-field XTEM image in the vicinity immediately under the Berkovich indent applied on single-crystal Si(100) with an indentation load of 200 mN

Si-III and Si-XII are clearly visible in the continuous load-unload cycle, consistent with the XTEM observations.

Nanoindentation on MOCVD-derived GaN Thin Films

GaN, a III–V wide-band-gap semiconductor, has received a great deal of attention in the recent years due to its potential for the realization of photonic devices such as laser and light emitting diodes (LEDs) operating in the ultraviolet portion of the electromagnetic spectrum as well as solar-blind photodetectors [30]. Its wide band gap, high breakdown field and, high electron saturation velocity also make it as an attractive candidate for the development of electronic devices operating at high temperature, high power and high frequency relative to other competing materials such as Si and GaAs [31, 32]. Consequently, majority of researches on this compound have been focused on exploring its optoelectronic characteristics. However, due to the ubiquitously existent lattice mismatch-induced stress between GaN thin films and the available substrates, the resultant defects have been found to significantly affect the threshold power density in stimulated emission of GaN optoelectronic devices. Therefore, it is becoming increasingly evident that research on the mechanical characteristics of GaN thin films is important to make GaN thin films to be a good candidate for electronic devices. In this work, the mechanical deformation of GaN thin films under Berkovich nanoindenter is examined. Such

knowledge is of great importance for realizing better manufacturing processes and devices stability.

Figure 4 displays the typical indentation load-displacement curve of GaN thin films subjected to a maximum indentation load of 200 mN. During loading, prominent multiple pop-ins, or sudden displacement excursions are triggered by discontinuous yielding from dislocation nucleation and motion. It can be found that the first apparent pop-in occurs at an indentation load about 80 mN. Subsequently, the multiple pop-ins are randomly distributed on the loading curve. According to the previous studies [3, 10], we note here that the critical applied indentation load for direct identification of the multiple pop-ins in the load-displacement curve is not only dependent on the type of indenters used, but also even very much dependent on the test systems and the maximum applied indentation loads used. Thus, we reasonably deduce that these discrepancies are mainly due to the various indentation methods used. For example, the tip-surface contact configuration and stress distribution for the Berkovich indenter tip can be drastically different from that for the spherical tip or Vickers-type indenters [3, 10; 33].

In addition, the multiple pop-ins behavior has been observed in materials with hexagonal structures such as sapphire [34], GaN [12] and single-crystal bulk ZnO [35], while for materials like InP and GaAs with the cubic structure only single pop-in event was observed [8]. Nevertheless, the above discussions do suggest that multiple pop-ins indeed are specific features of materials with the hexagonal lattice structure and, the geometry of the indenter tip may play an important role in determining the nanoindentation-induced mechanical responses. Thus, in order to identify the deformation mechanisms specific to the Berkovich nanoindentation direct microstructure characteristics in the vicinity of the indented area are needed.

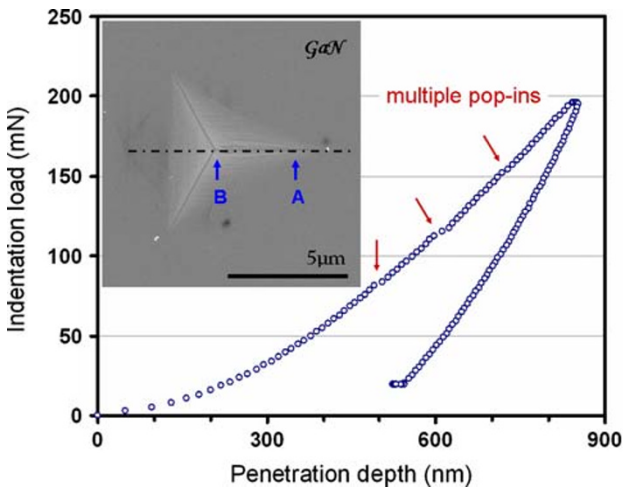

Fig. 4 Load-displacement data for GaN thin film obtained during nanoindentation with a Berkovich indenter showing "multiple pop-ins" (arrows) during loading. In addition, the inset is a SEM micrograph showing the indentation at an applied load of 200 mN

The inset of Fig. 4 displays the typical SEM micrograph for an indented surface obtained with the maximum applied indentation load of 200 mN. There is no evidence of dislocation activity or crack formation in the area of indented surface. Thus, if the dislocation nucleation and subsequent propagation are indeed the primary mechanism for the observed multiple pop-ins, it should prevail underneath the indented surface. It is also interesting to check if there is any pressure-induced phase transformation involved. At the ambient conditions, GaN tends to crystallize into the Wurtzite structure. However, theoretical studies [36, 37], which have been confirmed experimentally [38, 39], have predicted that, upon applying a hydrostatic pressure on the order of about 50 GPa, GaN will undergo the pressure-induced phase transformation into the Rocksalt structure. These values are significantly higher than the apparent room-temperature hardness of GaN thin films and the maximum load employed in this study. As will be presented in the followings, we used the micro-Raman spectroscopy and XTEM techniques in trying to clarify some of the issues concerning the nanoindentation-induced phase transformation in GaN thin films.

The micro-Raman spectra for Berkovich indenter operated at an indentation load of 200 mN are illustrated in Fig. 5. Three spectra are displayed—one before nanoindentation and the other two taken at different positions (corner and center of indent) after nanoindentation. The characteristic features of E_2^H and $A_1(LO)$ peaks, locating, respectively, at 568 cm^{-1} and 733 cm^{-1} are clearly observed in the pristine GaN thin film. As is evident from Fig. 5, both E_2^H and $A_1(LO)$ modes are shifted to the higher wavenumbers after Berkovich nanoindentation. The fact that the peak displacement is largest at the center of the indented area and decreases outward indicates that the compressive stresses might be the dominant factors. In addition, band broadening is revealed due to residual deformation via nanoindentation. We note that Puech et al. [40] also reported the similar shifts in micro-Raman results taken from point-indentation with an indentation load of 100 mN and had attributed these small shifts to residual compressive stress within the indented area. Finally, no extra peaks were observed in our micro-Raman spectra from nanoindentation, indicating that no phase transition in the material has occurred. Also, the SEM image of the same indentation area displayed in the inset of Fig. 4 does not reveal any characteristic of the pressure-induced metallization, either. We suspect that, in the film-substrate system, the indentation load applied to the film may have been partly absorbed by the substrate and distributed over a much larger area. Consequently, the local stress concentration beneath the indenter is significantly reduced to values insufficient for phase transformation to occur.

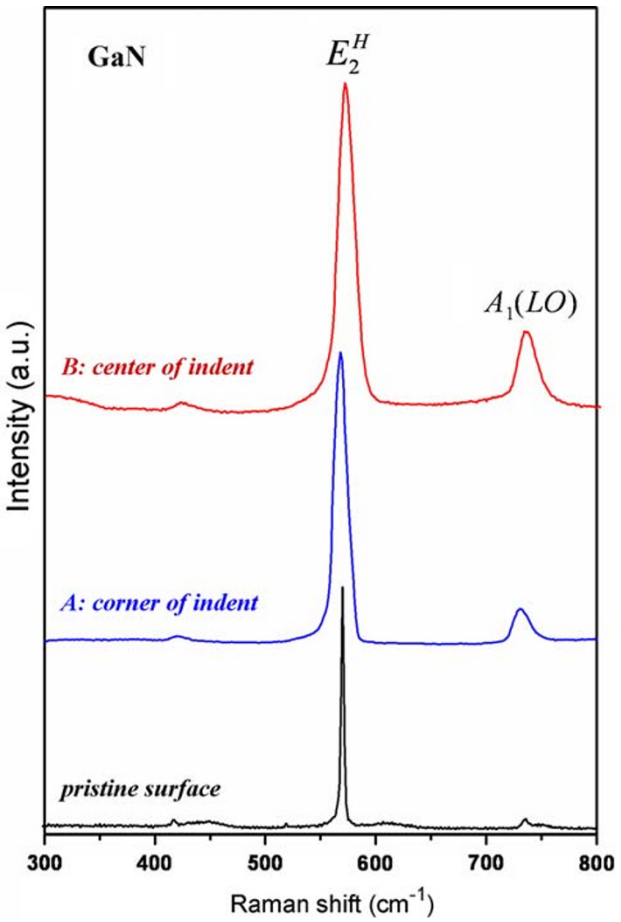

Fig. 5 Raman spectra of GaN thin film taken on the pristine surface and after nanoindentation (at the corner and center of indent). Changes in Raman spectra after indentation, though displaying the effects of compressive stress, do not show clear evidence of phase transformation. The inset of Fig. 4 shows the SEM micrograph of the same area after the Berkovich indentation on GaN thin film obtained at an indentation load of 200 mN. And, no cracking is evident to be responsible for the "multiple pop-ins" observed in the load-displacement curves

To further elucidate the nanoindentation-induced deformation, a bright-field XTEM image of an indentation load of 200 mN in GaN thin films is displayed in Fig. 6. The image clearly displays that, within the film, the deformation features underneath the indented spot are primarily manifested by dislocation activities. Namely the slip bands are well aligned in parallel with the {0001} basal planes all the way down to the film-substrate interface. Moreover, the picture clearly displays a typical microstructure of a heavily deformed material, characterized by features of very high density of dislocations. Nevertheless, the slip bands (dark thick lines in the photograph) clearly indicate that during the indentation the rapidly increasing dislocations can glide collectively along the easy directions. In the present case, in addition to those aligning parallel to the GaN-sapphire interface along the (0001) basal planes, slip bands oriented

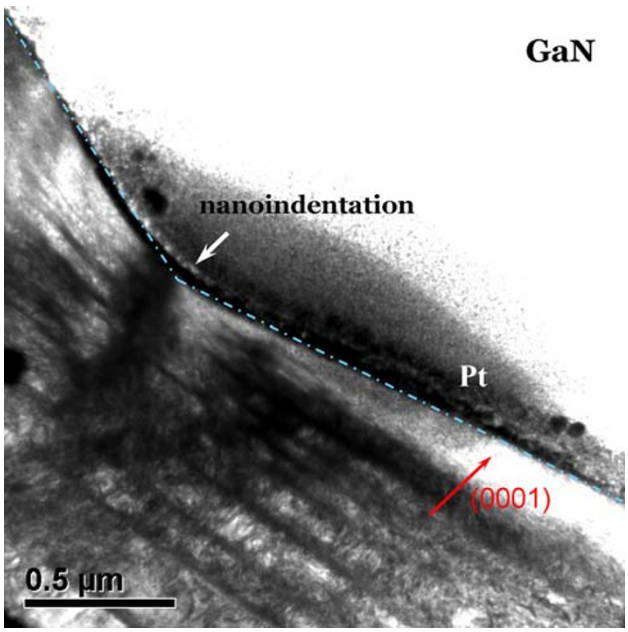

Fig. 6 The bright-field XTEM image in the vicinity immediately under the Berkovich indent applied on GaN thin film with an indentation load of 200 mN

at $\sim 60°$ to the sample surface can also be found. The 60° slip bands, which are believed to originate from dislocations gliding along the $\{10\bar{1}1\}$ pyramidal planes, however, distribute in much shallower regions near the contacting surface. It is indicative that much higher stress level is needed to activate this slip system as compared to the one along the basal planes. From Fig. 6, it can be seen that a more detailed microstructure near the intersections of the two sets of slip bands. The distorted slip bands and the extremely high dislocation densities at the intersections indicate highly strained state of the material. However, even at the submicron scale, no evidence of subsurface cracking and film fragmentation was observed. In addition, the selected area diffraction (not shown here) of the heavily damaged regions did not shown evidence of newly formed phases either.

In closing, it is apparent that, in the Berkovich indentation scheme, the primary deformation mechanism for GaN films is dislocation nucleation and propagation along easy slip systems, similar to that concluded with spherical indenter [12]. Since the multiple pop-ins are usually observed after permanent plastic deformation has occurred (80 mN in the present case) and two of the possible mechanisms, the deformation-induced phase transformation and fracture of thin films [41] were basically ruled out, the most likely mechanism responsible for the multiple pop-ins appears to be associated with the activation of dislocation sources [42]. In this scenario, plastic deformation prior to the pop-in event is associated with the individual movement of a small number of newly nucleated and pre-existing dislocations. As the number of dislocations

is increased and entangled to each other, large shear stress is quickly accumulated underneath the indenter tip. When the local stress underneath the tip reaches some threshold level, a burst of collective dislocation movement on the easy slip systems is activated, leading to a large release of local stress and a pop-in event on the load-displacement curve. Each of these collective dislocation movements is reflected as a slip band in the indented microstructure displayed in Fig. 6. Finally, we note that the so-called "slip-stick" behavior [12], characterized by material pile-ups caused by interactions between the as-grown defects and the indentation-induced dislocations, is not significant in this study. Whether it is due to the insignificant grown-in defect density of our GaN films or is related to the specific geometric shape of the indenter tip used is not clear at present and further studies may be required to clarify this issue.

Conclusions

In conclusions, a combination of nanoindentation, micro-Raman spectroscopy, FIB and TEM techniques has been carried out to investigate the contact-induced structural deformation behaviors in single-crystal Si(100) and MOCVD-deposited GaN thin films.

The micro-Raman analysis, measured from the indented materials which had plastically deformed on loading, showing a phase transformation occurs in Si whereas the results for GaN thin films do not give sufficient evidence for phase transformations. By using the FIB milling to accurately position the cross-section of the indented region, the XTEM results demonstrate that the major plastic deformation were taking place through the indentation-induced metastable phases (Si-III and Si-XII) and amorphous phase exhibited in Si, and the propagation of dislocations displayed in GaN thin films. Results revealed that the primary indentation-induced deformation mechanism in GaN thin films is nucleation and propagation of dislocations, rather than proposed stress-induced phase transformations or crack formations in Si via Berkovich nanoindentation.

Acknowledgements This work was partially supported by the National Science Council of Taiwan, under Grant No.: NSC 96-2112-M-214-001.

References

1. X.D. Li, B. Bhushan, Thin Solid Films **377–378**, 401 (2000)
2. X.D. Li, H. Gao, C.J. Murphy, K.K. Caswell, Nano Lett. **3**, 1495 (2003)
3. S.R. Jian, T.H. Fang, D.S. Chuu, J. Electron. Mater. **32**, 496 (2003)
4. S.R. Jian, T.H. Fang, D.S. Chuu, Appl. Surf. Sci. **252**, 3033 (2006)
5. X.J. Lu, X. Wang, P. Xiao, Thin Solid Films **494**, 223 (2006)
6. P. Xu, J.J. Li, Q. Wang, Z.L. Wang, C.Z. Gu, Z. Cui, J. Appl. Phys. **101**, 014312 (2007)
7. A. Mujica, A. Rubio, A. Muñoz, R.J. Needs, Rev. Mod. Phys. **75**, 863 (2003)
8. J.E. Bradby, J.S. Williams, J.W. Leung, M.V. Swain, P. Munroe, Appl. Phys. Lett. **78**, 3235 (2001)
9. J.E. Bradby, J.S. Williams, J.W. Leung, M.V. Swain, P. Munroe, Appl. Phys. Lett. **77**, 3749 (2000)
10. S.O. Kucheyev, J.E. Bradby, J.S. Williams, C. Jagadish, M. Toth, M.R. Phillips, M.V. Swain, Appl. Phys. Lett. **77**, 3373 (2000)
11. S.O. Kucheyev, J.E. Bradby, J.S. Williams, C. Jagadish, M.V. Swain, G. Li, Appl. Phys. Lett. **78**, 156 (2001)
12. J.E. Bradby, S.O. Kucheyev, J.S. Williams, J.W. Leung, M.V. Swain, P. Munroe, G. Li, M.R. Phillips, Appl. Phys. Lett. **80**, 383 (2002)
13. H. Olijnyk, S.K. Sikka, W.B. Holzopfel, Phys. Lett. A **103**, 137 (1984)
14. J.Z. Hu, L.D. Merkle, C.S. Menoni, I.L. Spain, Phys. Rev. B **34**, 4679 (1986)
15. J. Grain, G.J. Ackland, J.R. Maclean, R.O. Piltz, P.D. Hatton, D.S. Pawley, Phys. Rev. B **50**, 13043 (1994)
16. G. Weill, J.L. Mansot, G. Sagon, C. Carlone, J.M. Besson, Semicond. Sci. Technol. **4**, 280 (1989)
17. A. Kailer, K.G. Nickel, Y.G. Gogotsi, J. Raman Spectrosc. **30**, 939 (1999)
18. I. Zarudi, J. Zou, L.C. Zhang, Appl. Phys. Lett. **82**, 874 (2003)
19. D. Ge, V. Domnich, Y. Gogotsi, J. Appl. Phys. **93**, 2418 (2003)
20. S. Ruffell, J.E. Bradby, J.S. Williams, Appl. Phys. Lett. **89**, 091919 (2006)
21. M.M.O. Khayyat, D.G. Hasko, M.M. Chaudhri, J. Appl. Phys. **101**, 083515 (2007)
22. J.E. Bradby, J.S. Williams, J.W. Leung, M.V. Swain, P. Munroe, J. Mater. Res. **16**, 1500 (2001)
23. I. Zarudi, L.C. Zhang, M.V. Swain, Appl. Phys. Lett. **82**, 1027 (2003)
24. I. Zarudi, L.C. Zhang, J. Zou, T. Vodenitcharova, J. Mater. Res. **19**, 332 (2004)
25. V. Domnich, Y. Gogotsi, S. Dub, Appl. Phys. Lett. **76**, 2214 (2000)
26. A. Kailer, Y.G. Gogotsi, K.G. Nickel, J. Appl. Phys. **81**, 3057 (1997)
27. D.R. Clarke, M.C. Kroll, P.D. Kirchner, R.F. Cook, B.J. Hockey, Phys. Rev. Lett. **60**, 2156 (1988)
28. Y.G. Gogosti, V. Domnich, S.N. Dub, A. Kailer, K.G. Nickel, J. Mater. Res. **15**, 871 (2000)
29. I. Zarudi, L.C. Zhang, Tribol. Int. **32**, 701 (1999)
30. S.J. Pearton, J.C. Zolper, R.J. Shul, F. Ren, J. Appl. Phys. **86**, 1 (1999)
31. S.J. Pearton, F. Ren, A.P. Zhang, G. Dang, X.A. Cao, K.P. Lee, Mater. Sci. Eng. B. **82**, 227 (2001)
32. C.H. Oxley, Solid-State Electron. **48**, 1197 (2004)
33. K. Funato, F. Nakamura, S. Hashimoto, M. Ikeda, Jpn. J. Appl. Phys. **37**, L1023 (1998)
34. P. Kavouras, Ph. Komninou, Th. Karakostas, Thin Solid Films **515**, 3011 (2007)
35. R. Nowak, T. Sekino, S. Maruno, K. Niihara, Appl. Phys. Lett. **68**, 1063 (1996)
36. S.O. Kucheyev, J.E. Bradby, J.S. Williams, C. Jagadish, M.V. Swain, Appl. Phys. Lett. **80**, 956 (2002)
37. A. Munoz, K. Kunc, Phys. Rev. B **44**, 10372 (1991)
38. P.E. Van Camp, V.E. Van Doren, J.T. Devreese, Solid State Commun. **81**, 23 (1992)
39. H. Xia, Q. Xia, A.L. Ruoff, Phys. Rev. B **47**, 12925 (1993)

40. M. Ueno, M. Yoshida, A. Onodera, O. Shimomura, K. Takemura, Phys. Rev. B **49**, 14 (1994)
41. P. Puech, F. Demangeot, J. Frandon, C. Pinquier, M. Kuball, V. Domnich, Y. Gogotsi, J. Appl. Phys. **96**, 2853 (2004)
42. S.J. Bull, J. Phys. D: Appl. Phys. **38**, R393 (2005)
43. Y. Gaillard, C. Tromas, J. Woirgard, Phil. Mag. Lett. **83**, 553 (2003)